NUCLEAR THEORY, Vol. 40 (2023)
eds. M. Gaidarov, N. Minkov, Heron Press, Sofia

Monopole and Quadrupole Coupling in the Isoscalar Giant Resonances in ^{94}Zr and ^{96}Zr

M. El Adri, **Y. El Bassem**, **A. El Batoul**, **M. Oulne**

High Energy Physics and Astrophysics Laboratory, Department of Physics, Faculty of Sciences Semlalia, Cadi Ayyad University, P.O.B. 2390, Marrakesh, Morocco

Abstract. The isoscalar giant resonances for ^{94}Zr and ^{96}Zr are studied by the quasiparticle finite amplitude method based on the covariant density functional theory using the Density-Dependent Point-Coupling DD-PC1 and DD-PCX models. Validation of the numerical implementation is examined for ^{90}Zr and ^{92}Zr, then a good agreement with the available experimental isoscalar monopole strengths is obtained. The well-known monopole-quadrupole coupling that splits the isoscalar giant monopole resonance is identified in ^{94}Zr and ^{96}Zr isotopes. A soft monopole mode is found near 14.7 MeV for ^{94}Zr, and at 15.2 MeV for ^{96}Zr.

1 Introduction

Giant resonances [1,2] are collective excitations resulting from either the oscillation of nuclear density or nucleon motion induced by external fields or collisions. The most extensively studied types among these resonances are the isoscalar giant monopole resonance (ISGMR) [3, 4] which is considered as a compression mode of the nucleus, and the isoscalar giant quadrupole resonance (ISGQR). ISGQR occurs when the quadrupole vibration energy of the nucleus resonates with the excitation energy [5]. The initial identification of giant resonances in nuclei dates back to 1937 when Bothe and Gentner, as noted in [6], made the pioneering discovery. Later, in 1948, Goldhaber and Teller [7] proposed an interpretation of these resonances as the isovector giant quadrupole resonance (IVGDR).

By incorporating the Quasiparticle Finite Amplitude Method (QFAM) [8] within the framework of the Relativistic Hartree-Bogoliubov (RHB) model [9–11], the computational challenges associated with the Random Phase Approximation (RPA) method [12], are mitigated. This integration enables the exploration of excitation spectra and collective modes in nuclei with greater efficiency. As a result, it has yielded valuable insights into various phenomena, including giant resonances [13], pygmy dipole resonances [14], and soft monopole modes [15], thereby advancing our comprehension of nuclear structure and dynamics.

In this study, we have conducted calculations for the ground state and the distribution of giant resonances in Zr isotopes using the Quasiparticle Finite

Amplitude Method (QFAM) within the framework of the Relativistic Hartree-Bogoliubov (RHB) model. We have employed two different relativistic zero-range effective interactions, DD-PCX [16], and DD-PC1 [17], which exhibit distinct values for nuclear matter incompressibility.

The structure of this article is as follows: In Section 2, we provide a brief summary of the approaches employed for our calculations. Section 3 contains the numerical specifics, information about the interactions utilized in our calculations, and a presentation, analysis, and discussion of the results obtained. Finally, in Section 4, we present the main conclusions drawn from our work and provide an outlook for future research.

2 Theoretical Framework

The decay and the structural properties, as well as the excited states, not only of spherical but also of deformed nuclei can be successfully described by the Relativistic Hartree-Bogoliubov (RHB) approach. In such theory, the nuclear single-reference state is described by a generalized Slater determinant $|\Phi>$ that represents a vacuum with respect to independent quasiparticles. The quasiparticle operators are defined by the unitary Bogoliubov transformation, and the corresponding HartreeBogoliubov wave functions U and V are determined by the solution of the RHB equation:

$$\begin{pmatrix} h_D - m - \lambda & \Delta \\ -\Delta^* & -h_D^* + m + \lambda \end{pmatrix} \begin{pmatrix} U_k \\ V_k \end{pmatrix} = E_k \begin{pmatrix} U_k \\ V_k \end{pmatrix} . \quad (1)$$

Where h_D is the single-nucleon Dirac Hamiltonian, Δ denotes the pairing field, and U and V are Dirac spinors.

The starting point of quasiparticle finite amplitude method (QFAM) is the linear response equations [19]

$$(E_\mu + E_\nu - \omega)\, X_{\mu\nu}(\omega) + \delta H^{20}_{\mu\nu}(\omega) = -F^{20}_{\mu\nu}, \quad (2)$$

$$(E_\mu + E_\nu - \omega)\, Y_{\mu\nu}(\omega) - \delta H^{02}_{\mu\nu}(\omega) = -F^{02}_{\mu\nu}, \quad (3)$$

E_μ and E_ν are quasiparticle energies, $X_{\mu\nu}$ and $Y_{\mu\nu}$ are transition amplitudes corresponding to annihilating two quasiparticles $\mu\nu$ (labeled as 02) or to creating two quasiparticles $\mu\nu$ (labeled as 20), respectively, and δH is the induced Hamiltonian when the nuclear system is perturbed by the external field F with the frequency ω.

Finally, the function response reads

$$S(\hat{F}, \omega) = ImTr(f^\dagger \delta\rho(\omega)) \quad (4)$$

where $f^\dagger$ are the matrix elements of the operator $\hat{F}$.

The transition density can be defined by the following equation

$$\delta\rho_{tr}(\omega) = \frac{1}{\pi} ImTr(\delta\rho(\omega)) \quad (5)$$

3 Numerical Details

In the ground state calculations, the numerical details suggested in Refs. [10,11] are also followed here. The covariant density functionals DD-PCX [16] and DD-PC1 [17] are used. Such parameters are given in Table 1. The pairing correlation is treated with the separable pairing force in coordinate space which was proposed by Tian et al. [18]. The equations of motion for nucleons are solved in a triaxial-deformed harmonic oscillator basis where we have used a safe full anisotropic basis.

For QFAM calculations, to avoid the occurrence of singularities of Eqs. (2) and (3), we replace the frequency ω by $\omega + i\gamma$ with a small parameter γ, related to the Lorentzian smearing $\tau = 2^{\gamma}$ in relativistic quasipatricle RPA calculations [19]. The parameter η which induces a numerical difference is chosen as 10^{-6}, and will be used in all the following calculations.

Table 1. The parameter sets of DD-PCX [16] and DD-PC1 [17] interactions

Parameter	**DD-PCX** [16]	**DD-PC1** [17]
m (MeV)	939	939
a_s (fm^2)	-10.97924	-10.04616
b_s (fm^2)	-9.03825	-9.15042
c_s (fm^2)	-5.31301	-6.42729
d_s	1.37908	1.37235
a_v (fm^2)	6.43014	5.91946
b_v (fm^2)	8.87062	8.86370
c_v (fm^2)	0.0	0.0
d_v	0.65531	0.64025
K_0	213	230
m^*/m	0.559	0.580

3.1 Ground-state deformation

Figure 1 shows the potential energy curves (PECs) of Zr isotopes calculated using the DD-PC1 and DD-PCX functionals, with the constraint on the axial deformation parameter β. For each isotope, PECs are obtained by minimization of the absolute binding energy under the constraint of a fixed β. As one can see from Figure 1, the PECs obtained with DD-PC1 and DD-PCX functionals lead to the same quantitative outcome for $^{90-96}$Zr. Except for the magic nucleus ^{90}Zr, where the potential energy is relatively steep and the spherical minimum is well defined, the all other investigated isotopes look soft against deformation parameter with shallow potential energy, especially when the mass number A increases.

In ^{92}Zr nucleus, the ground-state fluctuates around the spherical state showing flatness in the potential energy curve, and for ^{94}Zr, the ground-state become

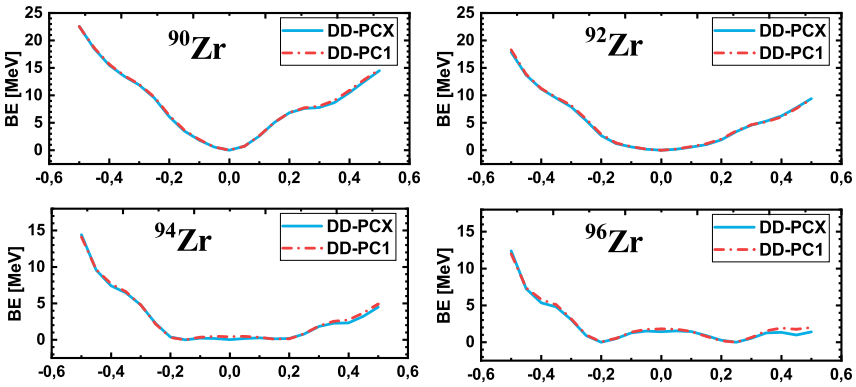

Figure 1. Potential energy curves obtained by constrained calculations with DD-PC1 and DD-PCX functionals.

almost prolate at $\beta = 0.2$ with an additional predicted minimum on the oblate side at $\beta = -0.2$. The same behaviour is observed for ^{96}Zr but with a potential barrier separating the two minima (prolate minima at $\beta = 0.25$ and oblate minima at $\beta = -0.2$), which shows that there is a coexistence between prolate and oblate shapes.

3.2 QFAM strength evolutions

In order to look for possible vibration properties peculiar to a modest axial deformation, we performed QRPA calculations for the Zr isotopes with the constraint β that corresponds to potential energy minimum in each studied nucleus. In Figure 2, the calculated strength functions of isoscalar giant monopole resonance (ISGMR), within DD-PC1 and DD-PCX functionals, for Zr isotopes are presented and compared to the available experimental data. For the prolate configuration, the obtained results within the two functionals exhibit that, in addition to the main ISGMR peak, a low-energy shoulder (so called also soft monopole mode) appears in ^{94,96}Zr. This structure gives a flat maximum in ^{96}Zr for the oblate case within the DD-PC1 parameterization, whereas the DD-PCX functional shows that ISGMR presents a single maximum.

Figure 2 displays that DD-PCX (K_0=213 and $m^*/m = 0.559$) reproduces the ISGMR data much better compared to DD-PC1 (K_0=230 and $m^*/m = 0.58$). It overestimates the experimental ISGMR peak energies by 1 MeV in ^{90}Zr and by 1.25 MeV in ^{92}Zr. For DD-PC1, the overestimate of peak energies are 2 MeV in ^{90}Zr and 2.35 MeV in ^{92}Zr. Thus the small value of K_0 and m^*/m are required to predict accurately the ISGMR.

To shed more light on the observed schedules in ^{94,96}Zr, we have displayed, in Figure 3, the ISGQR strength within the DD-PCX and DD-PC1 models. For both models the ISGQR peaks at 14.7 MeV in ^{94}Zr and at 15.2 MeV in ^{96}Zr. At the same points of energies, the ISGMR presents a low-energy shoulders.

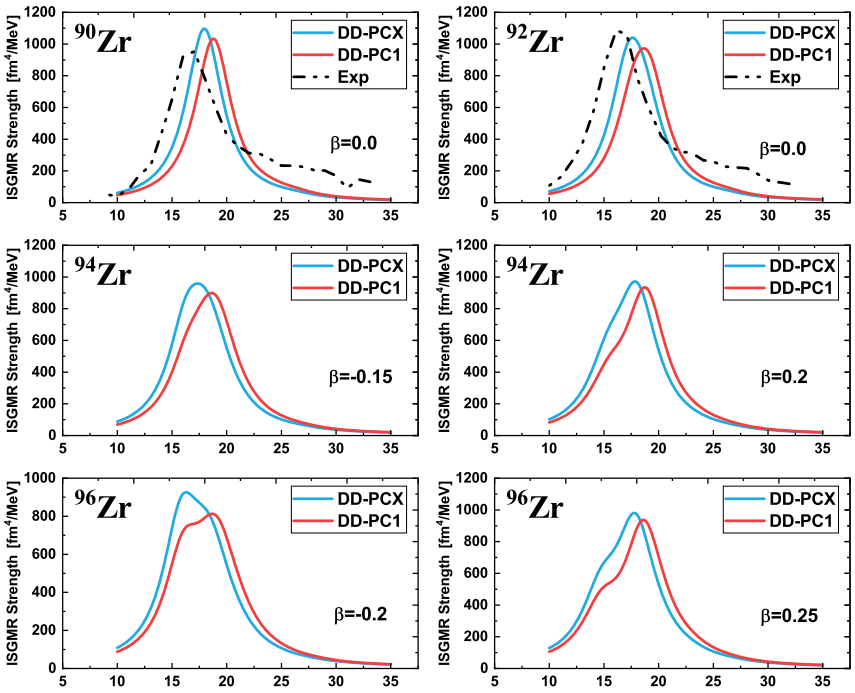

Figure 2. The calculated isoscalar monopole strengths in Zr isotopes, within DD-PC1 and DD-PCX models. The strengths are compared with the available experimental data.

This can be expalined by the deformation-induced coupling of the monopole and quadrupole modes.

In order to investigate the microscopic structure of the observed low-energy shoulders and to check which vibration dominates in ^{94,96}Zr, the transition densities in the (z,r) plan are calculated and illustrated in Figure 4. Using DD-PC1 and DD-PCX, the results are plotted near the soft monopole mode at ω =14.7 MeV for ^{94}Zr, and at ω =15.2 MeV for ^{96}Zr. The predicted root-mean-square

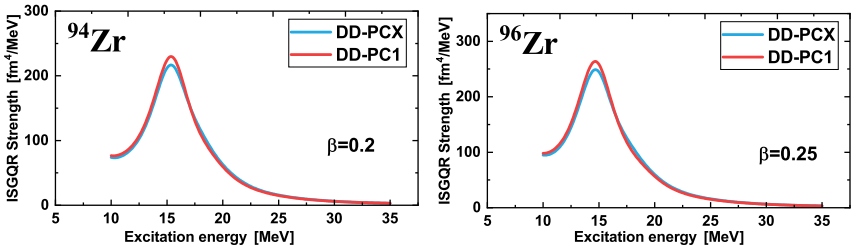

Figure 3. The calculated isoscalar quadrupole strengths in ^{94,96}Zr isotopes, using DD-PC1 and DD-PCX models.

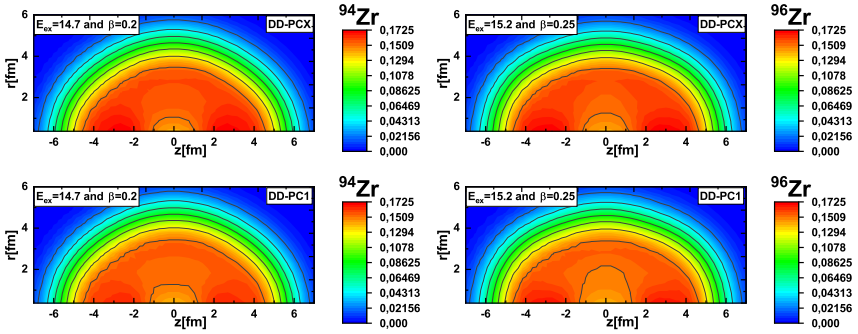

Figure 4. Transition densities of the soft monopole mode for ^{94,96}Zr isotopes in the prolate case using DD-PC1 and DD-PCX models.

radii of ^{94}Zr and ^{96}Zr are respectively 4.59 fm and 4.66 fm for DD-PCX, and 4.57 fm and 4.66 fm for DD-PC1. Due to the prolate deformation, the nucleons of both nuclei vibrate differently in the r-direction and in the z-direction. According to the above discussion, this can be also explained by the coupling between the ISGMR and ISGQR. In addition, the nucleons near the surface may vibrate in a different phase with respect to the nucleons in the core. The identified vibrations predominate in all cases in z-direction with high amplitude.

4 Conclusion

A systematic analysis of isoscalar giant monopole resonance strength in Zr isotopic chain, and especially of the coupling between the ISGMR and ISGQR, has been carried out within the framework of the quasiparticle finite amplitude method based on the deformed relativistic Hartree-Bogoliubov theory. For this purpose, two effective forces DD-PCX and DD-PC1, characterized by different values of incompressibility K_0 and Dirac mass ratio m^*/m, are selected.

We show that, in the ground state, for most investigated Zr isotopes, the potential energy curve (PEC) as a function of the deformation parameter β looks soft with shallow potential energy. Our QFAM calculations based on a deformed ground state reproduce the profile of the monopole strength distributions. In ^{94}Zr and ^{96}Zr, the monopole strength exhibits a main peak and a lower-energy shoulder near 15.7 MeV and near 14.7 MeV, respectively in both oblate and prolate cases. According to our interpretations, this shoulder is produced by the deformation-induced coupling of ISGMR and ISGQR.

It is also shown that DD-PCX functional with low value for K_0 and for m^*/m, reproduce better the ISGMR peak energies. We note, furthermore, that for the observed soft monopole modes, the neutron vibration occurs with a different phase near the surface region compared to the nucleons in the core.

References

[1] P. Chomaz, N. Frascaria: Multiple phonon excitation in nuclei: experimental results and theoretical descriptions. *Phys. Rep.* **135** (1995) 268.

[2] B.L. Berman, S.C. Fultz: Measurements of the giant dipole resonance with monoenergetic photons. *Rev. Mod. Phys.* **47** (1975) 713.

[3] S. Shlomo, P.J. Siemens: Isoscalar giant monopole in a macroscopic-microscopic approach. *Phys. Rev. C* **31** (1985) 2291.

[4] Y.K. Gupta, et al.: Deformation effects on isoscalar giant resonances in Mg 24. *Phys. Rev. C* **93** (2016) 044324.

[5] T. Kishimoto, et al.: Giant quadrupole resonance in deformed nuclei. *Phys. Rev. Let.* **35** (1975) 552.

[6] W. Bothe, W. Gentner: Atomumwandlungen durch-Strahlen. *Z. Physik* **106** (1937) 236248.

[7] M. Goldhaber, E. Teller: On nuclear dipole vibrations. *Phys. Rev.* **74** (1948) 1046.

[8] T. Nakatsukasa, T. Inakura, K. Yabana: Self-consistent calculation of nuclear photoabsorption cross sections: Finite amplitude method with Skyrme functionals in the three-dimensional real space. *Phys. Rev. C.* **76** (2007) 9 024318.

[9] J. Meng, H. Toki, S.G. Zhou, S.Q. Zhang, W.H. Long, L.S. Geng: Relativistic continuum Hartree-Bogoliubov theory for ground-state properties of exotic nuclei. *Prog. Part. Nucl. Phys.* **57** (2006) 470-563.

[10] M. El Adri, M. Oulne: Neutron shell closure at N = 32 and N = 40 in Ar and Ca isotopes. *Eur. Phys. J. Plus* **135** (2020) 268.

[11] M. El Adri, M. Oulne: Shell Evolution in Neutron-rich Ge, Se, Kr and Sr Nuclei within RHB Approach. *IJMPE* **29** (2020) 2050089.

[12] X. Sun, J. Chen, D. Lu: Pygmy dipole resonance built on the shape-isomeric state in ^{68}Ni. *Phys. Rev. C.* **98** (2018) 024607.

[13] H. Sasaki, K. Toshihiko, S. Ionel: Noniterative finite amplitude methods for E1 and M1 giant resonances. *Phys. Rev. C.* **105** (2022) 044311.

[14] D. Savran, T. Aumann, A. Zilges: Experimental studies of the pygmy dipole resonance. *Prog. Part. Nucl. Phys.* **70** (2013) 210-245.

[15] J.C. Pei, M. Kortelainen, Y.N. Zhang, F.R. Xu: Emergent soft monopole modes in weakly bound deformed nuclei. *Phys. Rev. C* **90** (2014) 051304.

[16] E. Yüksel, T. Marketin, N. Paar: Optimizing the relativistic energy density functional with nuclear ground state and collective excitation properties *Phys. Rev. C.* **99** (2019) 034318.

[17] T. Nikšić, D. Vretenar, P. Ring: Relativistic nuclear energy density functionals: Adjusting parameters to binding energies. *Phys. Rev. C.* **78** (2008) 034318.

[18] Y. Tian, Z.Y. Ma, P. Ring: A finite range pairing force for density functional theory in superfluid nuclei. *Phys. Lett. B.* **676** (2009) 44-50.

[19] A. Bjelčić, T. Nikšić: Implementation of the quasiparticle finite amplitude method within the relativistic self-consistent mean-field framework: The program DIRQFAM. *Comput. Phys. Commun.* **253** (2020) 107184.